Journal of Microscopy, Vol. 163, *Pt* 2, *August* 1991, *pp.* 117–130. ADONIS 002227209100095K
Received 2 *November* 1990; *revised* 20 *March* 1991; *accepted* 27 *March* 1991

Invited Review

An evanescent-field optical microscope

by N. F. VAN HULST, N. P. DE BOER *and* B. BÖLGER, *Opto-electronics, Applied Physics, University Twente, PO Box* 217, 7500 *AE Enschede, The Netherlands*

KEY WORDS. Scanning probe microscopy, (scanning) optical microscopy, nanometre-scale imaging, super-resolution, near field, evanescent field, attenuated/frustrated total internal reflection, optical antenna, light scattering

SUMMARY

The classic diffraction limit of resolution in optical microscopy ($\sim\lambda/2$) can be overcome by detecting the diffracted field of a submicrometre-size probe in its near field. The present stage of this so-called scanning near-field optical microscopy (SNOM) is reviewed.

An evanescent-field optical microscope (EFOM) is presented in which the near-field regime is provided by the exponentially decaying evanescent field caused by total internal reflection at a refractive-index transition. A sample placed in this field causes a spatial variation of the evanescent field which is characteristic for the dielectric and topographic properties of the sample. The evanescent field is frustrated by a dielectric probe and thus converted into a radiative field.

In our case the probe consists either of an etched optical fibre or of a highly sharpened diamond tip. The probe is scanned over the sample surface with nanometre precision using a piezo-electric positioner. The distance between probe and sample is controlled by a feedback on the detected optical signal. The resolution of the microscope is determined by both the gradient of the evanescent field and the sharpness of the tip. Details of the experimental set-up are discussed.

The coupling of the evanescent field to the submicrometre probe as a function of probe–sample distance, angle of incidence and polarization has been characterized quantitatively. The observed coupling is generally in agreement with presented theoretical calculations.

Microscopy has been performed on a regular latex sphere structure, which clearly demonstrates the capacity of the evanescent-field optical microscope for nanometre-scale optical imaging. Resolution is typically 100 nm laterally and 10 nm vertically.

The technique is promising for biological applications, especially if combined with optical spectroscopy.

INTRODUCTION

A light wave incident upon a sample is diffracted into both homogeneous and evanescent waves. In classical optical microscopy the homogeneous wave is detected and resolution is limited to *c.* $\lambda/2$ by diffraction. The evanescent wave, which contains

subwavelength information from the sample, is confined to the near field because it cannot propagate and can only be detected by a probe in the near field at a subwavelength distance from the sample.

The concept of near-field microscopy as a means to observe structural details smaller than the wavelength of the field itself goes back to O'Keefe (1956), who pointed out that if an illuminated subwavelength size aperture is scanned very close to an object the light detected in transmission contains structural information on the scale of the size of the aperture. Experimental evidence of the concept was given by Ash & Nicholls (1972), using microwave radiation. The renewed interest in optical near-field microscopy has been generated by the invention of the scanning tunneiling microscope (STM) by Binnig *et al.* (1982), as it provided the technology to scan a probe at nanometre scale over a sample surface. The near-field optical microscopic activities developed since are reviewed in the next section.

We report on an evanescent-field optical microscope (EFOM) in which the near-field regime is provided by the exponentially decaying evanescent field caused by total internal reflection at a refractive-index transition. A sample placed in this field causes spatial variations in the evanescent field which are characteristic of the dielectric and topographic properties of the sample. The evanescent field is frustrated by a dielectric probe tip and thus converted to a radiative field. An image is obtained by scanning the probe over the sample surface with nanometre precision by means of a piezo-electric positioner.

The experimental set-up of the EFOM is discussed in further detail. The measured signal variations are compared with theory and results are presented.

NEAR-FIELD OPTICAL MICROSCOPY: A REVIEW

The resolution of conventional optical microscopy is fundamentally limited by the diffraction limit, and therefore a major improvement would not be expected in imaging optical systems. Near-field microscopy completely avoids imaging optics. The optical electromagnetic field merely serves as a driving field, with a wavelength appreciably larger than the system, whereas the resolution is determined by a nanometre-size structure which serves as an optical antenna. An incident light beam diffracted at this antenna is strongly divergent with a high concentration close to its surface. The decay length is approximately equal to the dimensions of the microstructure. The spatial frequency spectrum of the field is dominated by correspondingly large wave numbers which represent the non-radiative evanescent waves. This is the near-field region. Spatial frequencies with small wave number are weakly present in the diffracted field. They represent the weak, but present, far-field radiation.

The distribution of the diffracted field is strongly sensitive to changes in the dielectric properties of the immediate surroundings of the antenna. A sample brought into the near-field region will modify the field distribution and the dielectric properties of the sample can be examined with a resolution corresponding to the antenna size.

The resolution of near-field microscopy is mainly limited by the capability of fabricating nanometre-size structures, by the ability to manipulate them on a nanometre scale and by the signal level. It is essentially impossible to illuminate a nanometre-size structure efficiently because an optical focus is limited to wavelength dimensions. Moreover, the far field of the diffracted light is detected, and this is only a small fraction of the driving field. Therefore resolution is improved at the expense of signal intensity.

A practical version of an SNOM consists of a microstructure, e.g. a sharp tip, an aperture in a thin film, or even a single particle, which is illuminated by a focused laser beam and the scattered far field detected. The optimum working distance in an SNOM is directly coupled to the resolution, so that a closed loop distance control is required

during operation. Similar to all scanning microscopic techniques the image is obtained by scanning the structure over a sample surface and collecting the signal as a function of position in a computer system with image processing capabilities.

The excitation wavelength is relatively unimportant with regard to the resolution of the system, yet it plays an important role in the dielectric properties of the sample under examination. The near-field distribution depends on the dielectric properties of its immediate environment (Ruppin, 1983), moreover nanometre-scale field enhancement may occur due to the lightning-rod effect at curved parts, and due to the excitation of a particle plasmon (Raether, 1977). Thus highly localized spectroscopic information, such as fluorescence or Raman scattering, is obtained, which can be enhanced by resonance effects for suitable wavelength and geometry.

A theoretical study of the near field of subwavelength apertures was started by Bethe (1944) and refined by Bouwkamp (1950a,b). A small circular aperture is assumed, with radius a, in a perfectly-conducting, infinitely-thin screen. The radius a is much smaller than the wavelength λ, and thus the time dependence of the system can be neglected in first approximation and the problem can be treated electrostatically. Bouwkamp (1950a,b) presented an exact solution for the electromagnetic field in and near to the aperture as a power series in the basic variable $ka = 2\pi a/\lambda$. Stimulated by the recent SNOM activities, Leviatan (1986) presented numerical results based on an equivalence principle in which he closed the aperture with a perfect conductor and provided for the original electric fields by attaching magnetic current sheets. Recently, Roberts (1989) performed exact numerical calculations, taking into account a finite screen thickness. The implications for expected signal level and contrast have been examined by Dürig *et al.* (1986). The results of the different theoretical approaches for a subwavelength aperture can be summarized as follows.

The near-field region

Within the hole the field intensity is almost constant, independent of the position, and proportional to k^2a^2, i.e. the area of the aperture. There are singularities at the edge of the aperture in directions associated with the polarization of the incident field, which cause the field intensity on the edges to be enhanced depending on the screen thickness. Throughout the near-field region the non-radiative evanescent waves are damped out and the field intensity decreases strongly with an r^{-4} dependence. The influence of a dielectric sample on the field distribution also decreases strongly in this regime. The radiation remains collimated to a distance of about the aperture radius. Thus, in this volume the field distribution is characteristic for the aperture. At greater distance the radiation diverges strongly and the width of the profile increases linearly with the distance. At a distance of about a wavelength the relationship to the aperture size is completely lost, because the source dimensions seem to be of the order of the wavelength itself. This is the transition to the far-field regime.

The far-field region

The far-field distribution is well described by the field of two sources, i.e. a magnetic dipole in the plane of the screen parallel to the polarization of the incident field and an electric dipole perpendicular to the screen parallel to the propagation direction of the incident beam. The emission perpendicular to the screen is dominated by the magnetic dipole radiation as expected for an aperture antenna (Lukosz & Kunz, 1977). The polarization is equal to that of the incident wave. The field intensity decreases quadratically (r^{-2}) with the distance, corresponding to a constant flux per steradian. The far-field flux is proportional to k^4a^6. This sixth power dependence on the aperture size implies a strong signal variation with slight changes in aperture size or sample absorption. Contrast is clearly strongly enhanced by this effect.

The fraction of the field energy in the hole that radiates into the far field is typically proportional to $(ka)^2$; this is only a small fraction, whilst the majority of the energy flows back and forth through the aperture. To obtain a quantitative idea of the signal intensity to be expected in the far field it should be remembered that it is only possible to focus about $(a/\lambda)^2$ of an optical beam onto the aperture and that the far-field flux is proportional to a^6. For example, when $a/\lambda = 0{\cdot}01$ about 10^{-10} of the incident flux would be expected in the far field.

Models which describe the interaction between a light-scattering microparticle and the evanescent field at a dielectric surface have recently been discussed by Vigoureux *et al.* (1989) and Labani *et al.* (1990).

Serious experimental studies of near-field optical effects were started by Lewis *et al.* (1984) at Cornell University, New York, Pohl *et al.* (1984) at the IBM research laboratories, Zürich and Fischer (1985) at MPI, Göttingen. Initially, subwavelength apertures as small as 30 nm were produced in conducting thin films, using lithographic techniques and electron beams. Contact near-field microscopy has been demonstrated using these films (Fischer, 1985; Betzig *et al.*, 1986). However, non-contact microscopy requires an aperture at the very end of a sharpened tip. Dürig *et al.* (1986) developed a technique to sharpen quartz tips up to 10 nm by proper polishing and ion milling; the quartz tips were metallized and an aperture was formed at the apex of the tip by cold deformation of the metal. Although 25 nm resolution was demonstrated, the lifetime of these tips was only a few hours. Betzig *et al.* (1986) fabricated metallized micropipettes with apertures as small as 50 nm, by pulling locally-heated glass rods; reproducible images of grating structures with 50 nm resolution were obtained using these pipettes (Betzig *et al.*, 1987).

Although initial schemes were set up in transmission, the system works just as well when source and detector are interchanged, as shown by Fischer *et al.* (1988) and Betzig *et al.* (1988). This more flexible reflection set-up enables microscopy of optically thick samples. In reflection the aperture is passed twice, which possibly enhances resolution and contrast. In principle the far-field flux will be equal for transmission and reflection as it is determined by the magnetic dipole radiation for both geometries.

The distance control in these systems was achieved by a tunnelling feedback loop between tip and sample. This yields a stability within 0·1 nm and a tuning range of a few nanometres. However, tunnelling is strictly limited to conductive samples, and as such seriously restricts the application of such a system. Fischer & Pohl (1989) demonstrated an alternative distance regulation with a feedback based on the characteristic decay of the optical signal. In this control mode the correction signal contains the information on the topographic and dielectric properties of the surface.

The potential of SNOM as a spectral probe technique was first demonstrated by Harootunian *et al.* (1986) in fluorescence mode and by Fischer (1986) and Fischer *et al.* (1987), who observed localized surface enhancement of fluorescence and scattering quenching.

Recently, the potential of the micropipettes was advantageously extended by Lieberman *et al.* (1990) by growing molecular-energy-confining crystals in the tip. Excitation of these nanometre-size crystals produces excitons which undergo a radiative decay, circumventing the cut-off criterion of propagation of light waves in the tip. Thus an ultra-small light source, ideally suitable for nanometre-scale imaging, was obtained.

The fabrication and short lifetime of subwavelength apertures remain the main problems. Fischer & Pohl (1989) have tried an interesting alternative: they replaced the aperture by a 100-nm latex sphere with an optically thin metal coating. With this probe they observed strong field enhancement which could possibly be attributed to surface plasmon effects, as suggested earlier by Wessel (1985). Recently, Fischer (unpublished

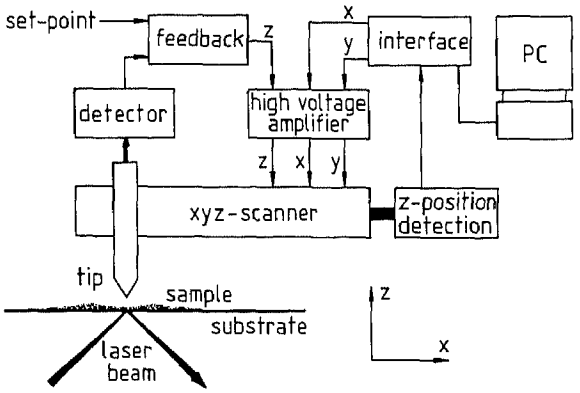

Fig. 1. Schematic set-up of the evanescent-field optical microscope.

data) suggested an optical coaxial line, i.e. an optical fibre with a metal core, which has the advantage that its size can be reduced to typically 50 nm without limitation of wave propagation by a cut-off criterion.

Although the principle of near-field optical microscopy has been convincingly demonstrated, the success story of the STM is not repeated and, as pointed out by Fischer (1990), 'the design of an SNOM in a reflection mode with a tip geometry remains a challenging task'.

An alternative, which completely circumvents the problem of aperture fabrication, has been developed by Reddick *et al.* (1989), Courjon *et al.* (1989), Sarayeddine *et al.* (1989), de Fornel *et al.* (1989), and our group, van Hulst *et al.* (1990), which is the subject of this paper. This is usually referred to as the photon scanning tunnelling microscope (PSTM) or evanescent-field optical microscope (EFOM). The evanescent field in this scheme does not originate from scattering but is generated by total internal reflection on a surface directly below the sample. This evanescent field is frustrated by a suitably sharpened dielectric probe and converted into a propagating wave. The coupling is efficient, in principle up to 100%, especially in comparison with a subwavelength aperture. A lateral resolution of 50–200 nm is observed, determined by the sharpness of the tip, the tip–sample distance and by the evanescent-field gradient as adjusted by the internal reflection angle.

DESCRIPTION OF THE EXPERIMENTAL SET-UP

The microscopic action of the EFOM takes place in the evanescent field at a refractive-index interface. A fraction of the field is coupled into a dielectric probe tip and the radiating field in the probe is focused onto a detector. The coupled signal depends exponentially on the probe–surface distance, similar to the tunnelling current in an STM. The exponential decay of the optical field allows the operation of a feedback system which maintains the optical signal at a constant level by adjusting the probe–surface distance by means of a piezo-electric actuator. A sample put on the glass surface will spatially modulate the evanescent field. The piezo-electric feedback action is a measure for the evanescent-field variation. An image is obtained by scanning the probe over the sample surface.

The experimental set-up is schematically sketched in Fig. 1. The evanescent field is generated by total internal reflection (TIR) of an HeNe laser beam ($\lambda = 632{\cdot}8$ nm, power = 8 mW) at a glass–air interface. The glass substrate (BK7, Schott) is highly polished up to $\lambda/20$ in order to minimize scattering effects and designed with the working surface horizontally and on the top side in order to be able to support liquid

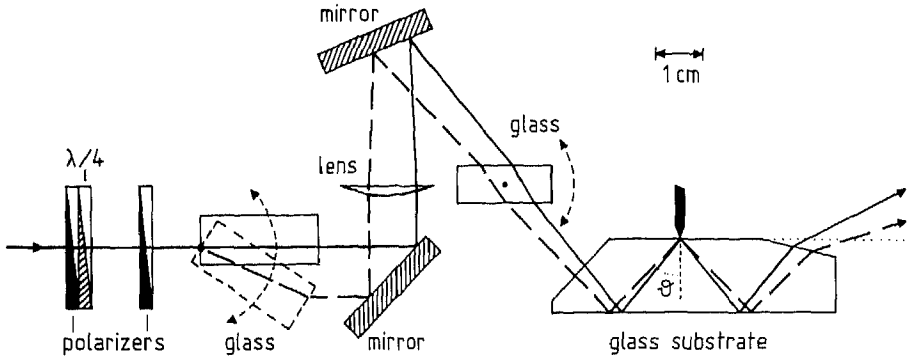

Fig. 2. Optical illumination path for internal reflection.

samples. Samples are prepared on a microscope cover slip which is placed on the glass substrate together with an index matching liquid.

Before entering the glass substrate the laser beam passes a polarizer and a wave plate which enable adjustment of the incident power and linear polarization direction (p or s polarization), as shown in Fig. 2. The beam is weakly focused at the TIR point to a diameter of 100 μm with 0·1° divergence. A rotatable plan-parallel glass plate before the focusing lens allows fine adjustment of the TIR angle of incidence, whereas a similar glass plate after the lens allows positioning of the TIR working area. The laser beam leaving the glass substrate after TIR is monitored in order to measure the angle of TIR.

Three different types of probe tips have been fabricated. (i) A quartz fibre (125 μm cladding, 50 μm core) is sharpened to about 200 nm with an apex of approximately 25° by chemical etching in an HF solution. Although fabrication is simple and reproducible, the fibre tips are very fragile and generally last for less than 1 day before degradation or destruction takes place. (ii) A diamond tip (Drukker Diamonds), $\phi = 1$ mm, with three polished facets intersecting at an apex of about 50 nm sharpness, is glued onto a graded index lens, as sketched in Fig. 3. The lens images the diamond apex onto an avalanche photo diode (APD). Thus a miniature probe system with a tip of high rigidity is obtained, which is relatively insensitive to stray light. (iii) A miniature diamond ruler (Drukker Diamonds), which is commercially used for engraving UV gratings, with largest dimension 170 μm, is glued onto the facet of a cleaved quartz fibre. Thus a simple and cheap probe construction is obtained with a tip of high rigidity.

The optical power coupled into the fibres is detected with a photo-multiplier tube (Hamamatsu R647-01); the power level is typically 0·1–1 nW and strongly dependent

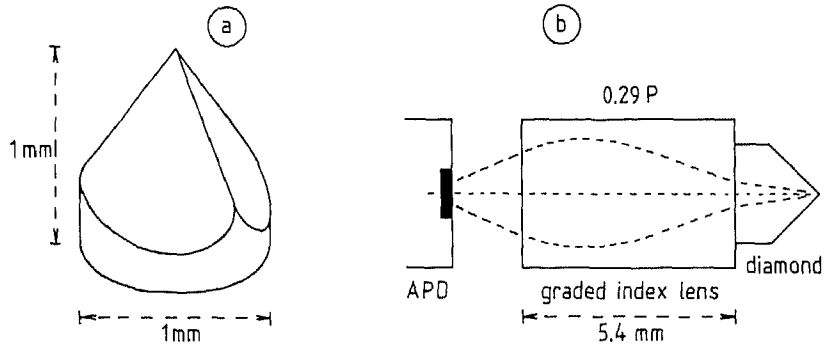

Fig. 3. (a) Polished diamond tip, apex angle = 90°. (b) Miniature integrated probe system with diamond tip.

on the coupling distance, the internal reflection angle and the tip shape. The optical probe tips can be manipulated in the x, y and z directions (see Fig. 1) over the sample surface by means of a Microblock (Photon Control) which combines rough mechanical positioning by differential drives (4-mm span, 0·1-μm accuracy) with fine piezo-electric scanning by multimorph elements (135-nm/V deflection, 22-μm span, 35-nm setting sensitivity). Due to its robust design the Microblock is rather flexible in the attachment of probes and its performance is not affected; on the other hand its lowest mechanical resonance frequency is about 200 Hz, resulting in rather slow scanning operation.

During a scan the optical signal is kept constant by a feedback system which consists of an integral, proportional, differential control unit and a high-voltage amplifier, which acts on the piezo-electric element in the z direction, similar to the 'tunnelling mode' of the STM. In principle the correction voltage on the piezo element contains the required microscopic information, but it also contains the hysteresis and the drift of the scanner. To circumvent this problem the height variations are monitored by an external opto-electronic system (Fig. 1). This system consists of a laser diode (Philips CQL63C) whose light beam passes through a pinhole (50 μm) and is directed onto a position-sensitive quadrant detector (RCA C30843E); the pinhole is attached to the scanner and consequently the quadrant detector difference signal gives a measure of the movement of the scanner. Typical short-time sensitivity of the system is 10 nm.

The total optical system is mounted on a vibration-isolated table with active damping. The microscope is controlled by an AT personal computer system with data-acquisition facilities (MetraByte Dash16 and DDA06). Thus scan patterns are generated, the signal is monitored and microscopic images are stored and processed.

THEORETICAL ASPECTS

The interest in the phenomenon of TIR dates back to the days of Newton and by now is very well documented (see, for example, Harrick, 1966). TIR occurs when light is incident from a dense medium (1) with high refractive index n_1 on a less-dense medium (2) with low refractive index $n_2 < n_1$ at an angle of incidence θ which is larger than the critical angle $\theta_c = \arcsin(n_2/n_1)$. The most fascinating aspect of TIR is that, although the reflection is total, energy is present beyond the boundary of TIR. Because the angle of transmission is purely imaginary, the electric field $\mathbf{E}_t(\mathbf{r})$ of the transmitted wave, represented by its propagation vector $\mathbf{k}_t$, can be written as

$$\mathbf{E}_t(\mathbf{r}) = \mathbf{E}_0\, e^{i(\omega t - \mathbf{k}_t \cdot \mathbf{r})} = \mathbf{E}_0\, e^{i(\omega t - k_x x)}\, e^{-z/d_p}, \tag{1}$$

where x and z are parallel and perpendicular to the interface, respectively, as indicated in Fig. 1, and d_p, the penetration depth, is given by

$$d_p = \frac{\lambda}{2\pi}(n_1^2 \sin^2\theta - n_2^2)^{-1/2}. \tag{2}$$

The parallel component of the incident wave travels along the boundary whilst the normal component decays exponentially. This inhomogeneous plane wave constitutes the evanescent-field regime which is the working region for the EFOM. The energy penetrating the rarer medium at a given place and time returns fully into the denser medium at another place and time; consequently, the net energy flow normal to the boundary is zero. The penetration into the rarer medium is typically one-tenth the wavelength for grazing incidence and increases to several wavelengths for incidence close to θ_c.

The amplitude reflection coefficient r for the reflected wave can be written as

$$r = e^{i\delta}. \tag{3}$$

The amplitude of the wave is not affected by the reflection ($|r| = 1$) while a phase shift δ occurs given by

$$\mathrm{tg}(\delta_s/2) = \frac{(n_1^2 \sin^2\theta - n_2^2)^{1/2}}{n_1 \cos\theta} \tag{4}$$

$$\mathrm{tg}(\delta_p/2) = \frac{n_1^2}{n_2^2}\,\mathrm{tg}(\delta_s/2) \tag{5}$$

for s and p polarization, respectively.

The exponentially decaying wave can be converted to a radiating wave by bringing a third dielectric medium with refractive index n_3 within a few penetration depths of the first medium. The reflectivity is reduced, resulting in frustrated total reflection (FTR), while power is transmitted to the third medium without loss at the interfaces. This is often referred to as 'optical tunnelling'. The theory has been described by, for example, Court & von Willisen (1964). The case of two semi-infinite media 1 and 3 can be analytically evaluated using complex Fresnel coefficients and the Stokes relationship. A straightforward calculation of the transmission $T(z)$ from medium 1 to medium 3 separated by a distance z for the case $n_1 = n_3$ yields

$$T(z)^{-1} = 1 + \frac{\sinh^2(z/d_p)}{\sin^2(\delta)}, \tag{6}$$

where δ is δ_s or δ_p depending on the polarization of the incident beam.

The calculated variation in transmission with spacing, according to Eq.(6), for several angles $\Delta\theta = \theta - \theta_c$ relative to the critical angle, both for p and s polarization, is drawn in Fig. 4. For large separation z the transmission decays exponentially proportional to $\exp(-2z/d_p)$, which corresponds to the intensity of the undisturbed evanescent field. For small separation ($z \ll d_p$) the evanescent field is highly disturbed and levels off towards 100% transmission. The coupling distance increases rapidly with decreasing $\Delta\theta$; however, unlike the penetration depth it does not grow to infinity as $\Delta\theta$ approaches zero. It should be noted that for small $\Delta\theta$ the coupling is larger for p than for s polarization, whilst for larger angles, typically $\Delta\theta > 10°$, the reverse is true. This is due to the fact that the phase shift, which changes from 0 to π with increasing $\Delta\theta$, increases faster for p than for s polarization; the coupling efficiency for both polarizations switches at the angle of incidence for which $\delta_p + \delta_s = \pi$.

For the case of a sharp dielectric tip, with a tip radius appreciably smaller than λ, as in our experiment, Eq. (6) is no longer valid. The complex Fresnel coefficients have to be taken into account for both interfaces, together with a coupling angle related to the tip shape. Because of the propagation in the x direction, coupling will only occur on one side of the tip. Moreover, the influence of a sample with variation in topographic and dielectric properties must be taken into account. A theoretical analysis taking into account surface corrugation was recently presented by Labani *et al.* (1990).

The resolution for scanning microscopy is determined by the size of the coupling region, which is a function of tip sharpness, evanescent-field gradient and polarization of the incident field.

Mathematically there is an analogy between the field coupling for FTR and the tunnelling of electrons through a quantum mechanical barrier, although the fundamental physical situations as described by the Maxwell and Schrödinger equations, respectively, are of different origin. From the experimental point of view the analogy also extends to the essential quality of STM: the exponential decay of the coupling enables feedback regulation and implies a resolution better than the overall tip sharpness.

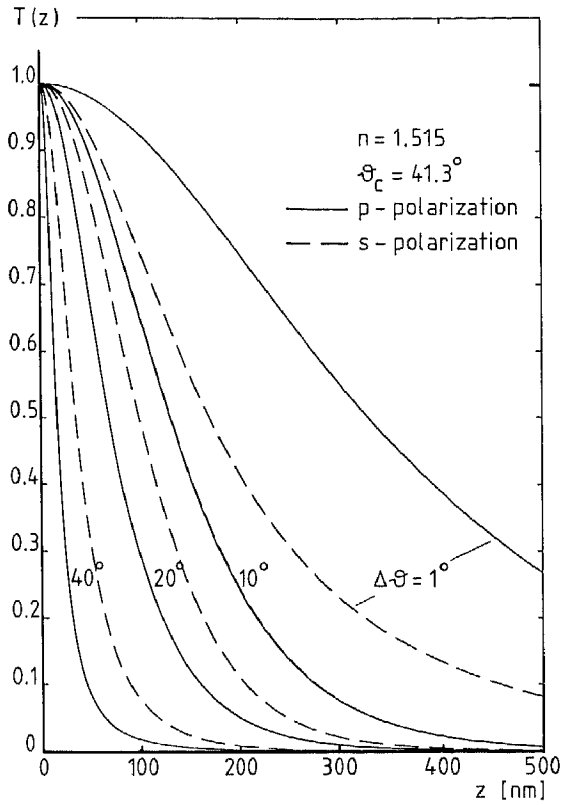

Fig. 4. Fraction of coupled light according to Eq.(6) as a function of distance at several angles $\Delta\theta = \theta - \theta_c$, for p polarization (solid curves) and s polarization (dashed curves).

RESULTS

In order to verify the basic concepts of the EFOM the optical signal coupled from a clean glass (BK7) substrate into the probe tip has been investigated as a function of the separation z between tip and substrate, the angle $\Delta\theta$ and the polarization. During the variation of parameters the feedback loop was kept continuously active. The z dependence of the coupling was determined by monitoring the z position as a function of the set point of the feedback, whereas the angle dependence was investigated by rotating the plan-parallel glass plate before the focusing lens.

The measured coupling signal as a function of z is shown in Fig. 5 for $\Delta\theta = 0{\cdot}55$–$1{\cdot}30°$ and p polarization. The minimum value of z was taken at a safe distance from the substrate, typically 0·5 μm. The curves display an exponential decay with z, and a strong decrease with increasing $\Delta\theta$. At these large distances the coupling for p polarization was slightly better, by a factor of about 1·5, than for s polarization. For decreasing separation between tip and surface the polarization effect becomes more pronounced. The measured effect of polarization is shown in Fig. 6 for $\Delta\theta = 0{\cdot}8°$. The curves extend towards the tip–surface contact. In this regime the signal levels off to a constant value. The exact position at which $z = 0$ is difficult to define because an approach ending in contact is often irreversible and because the feedback action is impossible if the optical signal is about constant as a function of distance. Directly outside the contact region the signal for p polarization is about twice that for s polarization ($\Delta\theta \simeq 0{\cdot}8°$).

The microscopic abilities of the EFOM have been examined with well-defined latex

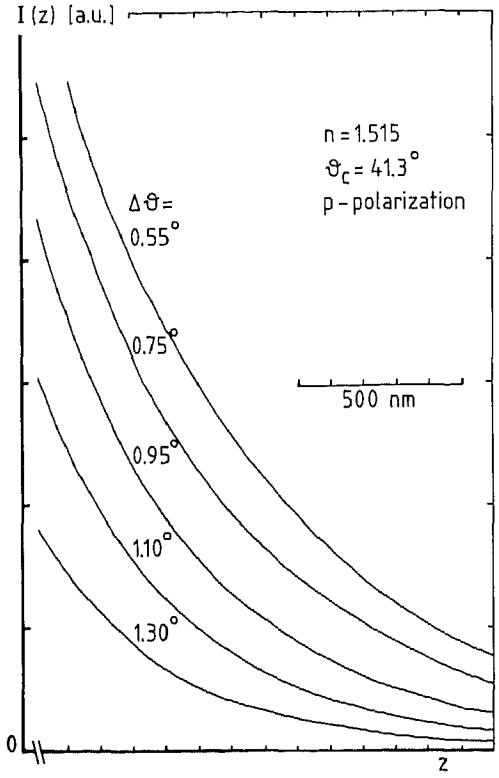

Fig. 5. Observed optical coupling $I(z)$ as a function of distance for several angles $\Delta\theta = \theta - \theta_c$.

spheres as test samples. A solution of latex spheres in water and methanol was evaporated on a cover slip. This test sample was placed on the glass substrate with an immersion liquid. The presence of the sample causes considerable scattering at the internal reflection point. Fortunately, the scattering light is mainly directed parallel to the incident beam, whereas the evanescent field extends normal to the surface. The coupling of scattered light can be largely reduced by placing the probe tip at a suitable angle to the surface normal. Moreover, the probe tips exhibit a limited acceptance angle, and scattering from sources in the vicinity of the probe region is only detected at larger separations ($z > 1$ μm) (van Hulst *et al.*, 1990).

An EFOM image of a 2×2-μm area of latex spheres with a 481-nm diameter is displayed in Fig. 7, both topographically and in grey scale. The image displays the directly measured optical coupling variations without further filtering or smoothing of the data. The spheres, which can be clearly distinguished, are closely packed because the image was taken at the edge region of a droplet of solution, where the spheres tend to concentrate. The microscopic resolution is typically 100 nm laterally and 10 nm vertically. The total height variation in Fig. 7 is 180 nm.

DISCUSSION

The fraction of the laser power coupled into the optical probe by FTR is typically 10^{-7}. This fraction is mainly determined by the ratio between the probe tip area ($\phi \simeq 100$ nm) and the waist ($\phi \simeq 100$ μm) of the laser beam focus. Taking this into account, typically 10% of the light power incident in the probe regime is coupled into the optical probe and indeed 100% is expected for contact (assuming $n_1 = n_3$).

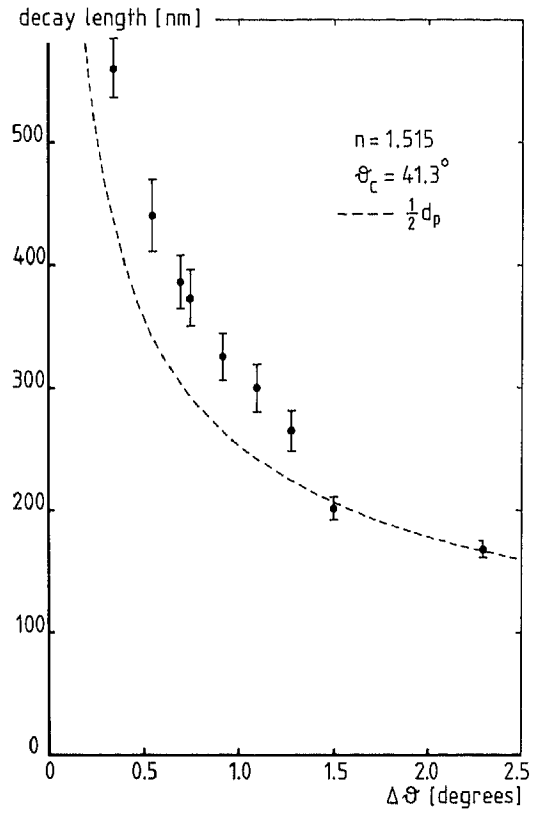

Fig. 8. Decay length of the optical coupling at large distance, experimental (dots) and theoretical (dashed curve).

From the measured exponential decay of the coupled signal at large z a decay length can be deduced. The measured decay length is plotted in Fig. 8 for several values of $\Delta\theta$. Theoretically a decay length of $d_p/2$ is expected both from Eq.(1) and Eq.(6), for large z; this value is also drawn in Fig. 8. The correspondence is reasonable, especially in view of the fact that the experimental values have been obtained with different tips. A similar correspondence was observed by Reddick *et al.* (1989) for both coated and uncoated fibres. The deviation of our experimental data from the theoretical curve for small $\Delta\theta$ can be attributed to a systematic uncertainty in $\Delta\theta$, which is measured relative to θ_c, and to the fact that the laser beam diverges at an angle of 0·1°.

The measured effect of polarization at large distance is weak, which corresponds to the situation that the evanescent field is only slightly disturbed, and indeed no polarization effect is expected. In contrast to the observed effect Eq.(6) predicts a ratio of $(n_1/n_2)^4$ for the coupling of p polarization to s polarization at large distance z and small $\Delta\theta$. This again stresses the fact that Eq.(6) does not apply for large distances.

For small z the measured optical coupling (Fig. 6) shows good agreement with the predicted behaviour according to Eq.(6) (Fig. 4), both in the levelling off in the contact regime and in the effect of polarization. A full quantitative comparison is difficult because of the uncertainty in the position at which $z = 0$.

Although our EFOM images clearly display subwavelength resolution and correspond to the expected structure of the sample, a quantitative analysis of the images is still at the initial stage. This requires more systematic imaging of periodic and non-

periodic samples at different values of z and $\Delta\theta$ and further development of a theoretical basis, as initiated by Labani *et al.* (1990).

In our present set-up, vertical resolution is limited to 10 nm and sampling of a complete image takes about 5 min. Both can be improved by a more compact set-up and a different scanner, for example a piezo tube scanner as conventionally used for STM.

The scattered light from the sample is an important drawback as it may even render the feedback action impossible. This is a fundamental problem in the application of the EFOM which can only be circumvented by discriminating the evanescent field against the stray light. A possible solution lies in the modulation of the angle of incidence by wobbling the plan-parallel glass plate or in the modulation of the polarization and subsequent phase-sensitive detection; both will modulate the penetration depth whilst the stray light is expected to remain roughly constant.

CONCLUSIONS

The observed local coupling corresponds quantitatively to the theoretical characteristics for frustrated TIR.

Our results clearly demonstrate the capacity of the EFOM to obtain subwavelength resolution. The resolution is determined not only by the sharpness of the probe tip but also by the exponential decay of the evanescent field itself, which can be controlled by changing the angle of incidence, working distance and wavelength.

EFOM images display variation in topography, refractive index and absorption. These can be disentangled by comparing scans at different height and must be confronted with a more quantitative theory.

The technique seems very promising for biological samples, especially when combined with spectroscopic techniques.

Construction of an EFOM that operates in reflection and can cope with scattering objects will be the next stage of this research.

ACKNOWLEDGMENTS

The technical assistance of F. B. Segerink has been essential to this work. The contribution of J.-C. Martinez-Antón to the characterization of the EFOM is greatly appreciated.

REFERENCES

Ash, E.A. & Nicholls, G. (1972) Super-resolution aperture scanning microscope. *Nature*, **237**, 510–513.

Bethe, H.A. (1944) Theory of diffraction by small holes. *Phys. Rev.* **66**, 163–182.

Betzig, E., Isaacson, M., Barshatzky, H., Lewis, A. & Lin, K. (1988) Super-resolution imaging with near-field scanning optical microscopy (NSOM). *Ultramicroscopy*, **25**, 155–164.

Betzig, E., Isaacson, M. & Lewis, A. (1987) Collection mode near-field optical microscopy. *Appl. Phys. Lett.* **51**, 2088–2090.

Betzig, E., Lewis, A., Harootunian, A., Isaacson, M. & Kratschmer, E. (1986) Near-field scanning optical microscopy (NSOM). *Biophys. J.* **49**, 269–279.

Binnig, G., Rohrer, H., Gerber, Ch. & Weibel, E. (1982) Surface studies by scanning tunneling microscopy. *Phys. Rev. Lett.* **49**, 57–61.

Bouwkamp, C.J. (1950a) On Bethe's theory of diffraction by small holes. *Philips Res. Rep.* **5**, 321–332.

Bouwkamp, C.J. (1950b) On the diffraction of electromagnetic waves by small circular disks and holes. *Philips Res. Rep.* **5**, 401–422.

Courjon, D., Sarayeddine, K. & Spajer, M. (1989) Scanning tunneling optical microscopy. *Opt. Comm.* **71**, 23–28.

Court, I.N. & von Willisen, F.K. (1964) Frustrated total internal reflection and application of its principle to laser cavity design. *Appl. Opt.* **3**, 719–726.

Dürig, U., Pohl, D.W. & Rohrer, F. (1986) Near-field optical scanning microscopy. *J. Appl. Phys.* **59**, 3318–3327.

Fischer, U.Ch. (1985) Optical characteristics of 0·1 μm circular apertures in a metal film as light sources for scanning microscopy. *J. Vac. Sci. Technol.* **B3**, 386–390.

Fischer, U.Ch. (1986) Sub micron aperture in a thin metal film as a probe of its micro environment through enhanced light scattering and fluorescence. *J. Opt. Soc Am. B*, **3**, 1239–1244.

Fischer, U.Ch. (1990) Resolution and contrast generation in scanning near-field optical microscopy. *Scanning Tunneling Microscopy and Related Methods* (ed. by R. J. Behm), pp. 475–496. Kluwer Academic Publishers, The Netherlands.

Fischer, U.Ch., Dürig, U. & Pohl, D.W. (1987) Near-field optical scanning microscopy and enhanced spectroscopy with submicron apertures. *Scanning Microsc. Suppl.* **1**, 47–52.

Fischer, U.Ch., Dürig, U.T. & Pohl, D.W. (1988) Near-field optical scanning microscopy in reflection. *Appl. Phys. Lett.* **52**, 249–251.

Fischer, U.Ch. & Pohl, D.W. (1989) Observation of single-particle plasmons by near-field optical microscopy. *Phys. Rev. Lett.* **62**, 458–461.

de Fornel, F., Goudonnet, J.P., Salomon, L. & Lesniewska, E. (1989) An evanescent field optical microscope. *Proc. SPIE*, **1139**, 77–84.

Harootunian, A., Betzig, E., Isaacson, M. & Lewis, A. (1986) Super-resolution fluorescence near-field scanning optical microscopy. *Appl. Phys. Lett.* **49**, 674–676.

Harrick, N.J. (1966) Principles of internal reflection spectroscopy. *Internal Reflection Spectroscopy* (ed. by John Wiley & Sons), pp. 13–66. Interscience Publishers, New York.

van Hulst, N.F., de Boer, N.P. & Bölger, B. (1990) Scanning near field optical microscopy. *Trans. Roy. Microsc. Soc.* **1**, 239–242.

Labani, B., Girard, C., Courjon, D. & Van Labeke, D. (1990) Optical interaction between a dielectric tip and a nanometric lattice: implications for near-field microscopy. *J. Opt. Soc. Am. B*, **7**, 936–943.

Leviatan, Y. (1986) Study of near-zone fields of a small aperture. *J. Appl. Phys.* **60**, 1577–1583.

Lewis, A., Isaacson, M., Harootunian, A. & Muray, A. (1984) Development of a 500 Å spatial resolution light microscope. *Ultramicroscopy*, **13**, 227–232.

Lieberman, K., Harush, S., Lewis, A. & Kopelman, R. (1990) A light source smaller than the optical wavelength. *Science*, **247**, 59–61.

Lukosz, W. & Kunz, R.E. (1977) Light emission by magnetic and dielectric dipoles close to a plane interface. *J. Opt. Soc. Am.* **67**, 1607–1619.

O'Keefe, J.A. (1956) Resolving power of visible light. *J. Opt. Soc. Am.* **46**, 359.

Pohl, D.W., Denk, W. & Lanz, M. (1984) Optical stethoscopy: image recording with resolution $\lambda/20$. *Appl. Phys. Lett.* **44**, 651–653.

Raether, H. (1977) Surface plasma oscillations and their applications. *Physics of Thin Films* (ed. by G. Hass, M. Francombe and R. Hoffman), Vol. 9, pp. 145–261. Academic Press, New York.

Reddick, R.C., Warmack, R.J. & Ferrell, T.L. (1989) New form of scanning optical microscopy. *Phys. Rev. B*, **39**, 767–770.

Roberts, A. (1989) Near-zone fields behind circular apertures in thick, perfectly conducting screens. *J. Appl. Phys.* **65**, 2896–2899.

Ruppin, R. (1983) Surface modes and optical absorption of a small sphere above a substrate. *Surf. Sci.* **127**, 108–118.

Sarayeddine, K., Courjon, D. & Spajer, M. (1989) Scanning tunneling optical microscopy (STOM) using a stylus sensor application to topography analysis of guiding surfaces. *Proc. SPIE*, **1139**, 68–72.

Vigoureux, J.M., Girard, C. & Courjon, D. (1989) General principles of scanning tunneling optical microscopy. *Opt. Lett.* **14**, 1039–1041.

Wessel, J. (1985) Surface-enhanced optical microscopy. *J. Opt. Soc. Am.* **B2**, 1538–1540.